

# Steady-state electron transport within InAlN bulk ternary nitride, using the Monte Carlo method

Nadia Bachir<sup>1</sup>, Abdelkader Hamdoune<sup>2</sup>, Nasr Eddine Chabane Sari<sup>3</sup>

Faculty of Science, University of Abou-bekr BELKAID, Unity of Research Materials and Renewable Energies, Tlemcen. ALGERIA

## Email address:

nadia\_bachir@hotmail.com (N. Bachir), a.hamdoune@gmail.com (A. Hamdoune), nechabaesari@yahoo.fr (N. E. C. Sari)

## To cite this article:

Nadia Bachir, Abdelkader Hamdoune, Nasr Eddine Chabane Sari. Steady-State Electron Transport within InAlN Bulk Ternary Nitride, using the Monte Carlo Method. *International Journal of Materials Science and Applications*. Vol. 3, No. 2, 2014, pp. 20-24.

doi: 10.11648/j.ijmsa.20140302.12

**Abstract:** Al-bearing III-nitride semiconductor materials are essential for the development of high-frequency and high-power electronic devices and optoelectronic devices operating in the ultraviolet spectral region, because of their wide band gap and unique electronic characteristics. The InAlN alloy is attracting much attention, due to its lattice matching capability to GaN substrates or buffer layers and its variable band gap energy which can be changed from 1.9 to 6.2 eV [1]; it can potentially be used for the fabrication of advanced electronic and optoelectronic devices. AlGaIn is being replaced by InAlN which is more advantageous and possesses quite remarkable properties. Unlike AlGaIn which, for example, in its use in HEMT structures is in high stress, InAlN can be used in its unstressed state. Thus, the generation of defects introduced by the constraints is greatly reduced. This has the advantages of limiting the electrical performance degradation associated with the presence of such defects and improving the reliability of the material. In this work, the ternary compound  $\text{In}_x\text{Al}_{1-x}\text{N}$  in the stationary mode is studied, using the Monte Carlo simulation method. The steady-state electron drift velocity is investigated for different mole fractions of indium in the alloy, for various temperatures. The same calculation is performed at 300K for AlGaIn and InGaIn alloys, in order to compare them.

**Keywords:** Aluminum Nitride (AlN), Indium Nitride (InN), Aluminum Indium Nitride InAlN, Stationary Mode, Monte Carlo Simulation Method

## 1. Introduction

Like all III-V compounds, the III-nitride compounds were very early synthesized and studied. The first GaN single-crystal was epitaxially grown on a sapphire substrate using the halide vapor phase epitaxy (HVPE). The large band gap of GaN and its possibility of alloying with AlN and InN have quickly raised great hopes for these materials as transmitters or detectors of visible or ultraviolet light (UV) [2].

In this work, the electron transport in the  $\text{Al}_x\text{In}_{1-x}\text{N}$  alloy is studied. This alloy is drawing much attention because at  $x = 0.18$ , it can be lattice-matched to GaN [3], and may be used in containment barrier optoelectronic structures based on nitrides. It is important to know its properties and have a good control of its growth objectives in order to develop new components, particularly in the far UV.

To a first approximation, the  $\text{In}_x\text{Al}_{1-x}\text{N}$  lattice constants, the effective masses, the mechanical and Varshni coefficients can be deduced from those of InN and AlN by linear interpolation, using the Vegard law.

$$a_{\text{In}_x\text{Al}_{1-x}\text{N}} = x \times a_{\text{InN}} + (1 - x) \times a_{\text{AlN}} \quad (1)$$

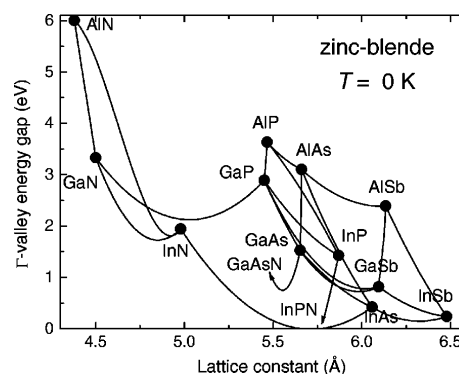


**Figure 1.** The gap energy as a function of the lattice constant of the different cubic compounds at  $T = 0 \text{ K}$  [2]

To study the electron transport, it is essential to know the band gap energy of the studied compounds. AlN has a larger gap and a smaller lattice constant than InN, as seen in Figure 1 [4].

The variation of the band gap energy of the alloy with respect to its composition is not linear but quadratic (Eq.2).

$$E_{In_xAl_{1-x}N}^g = x X E_{InN}^g + (1-x)X E_{AlN}^g - x(1-x)X b \quad (2)$$

In our alloy, this standard quadratic expression does not fit the compositional variation of the band gap very well. Guo *et al.* [5] and Kim *et al.* [6] subsequently presented the results for InN-rich and AlN-rich InAlN, respectively, which indicated a somewhat weaker bowing. Peng *et al.* gave a cubic expression for the energy gap, based on results over the entire range of compositions. A similar large bowing was observed by Yamaguchi *et al.* On the theoretical side, a first-principles calculation for zinc blend InAlN yielded a bowing parameter of 2.53 eV, which is assumed to be equal to that in the wurtzite alloy [6]. The most trustworthy quantitative report among these appears to be that of Peng *et al.* However, the suggested expression  $E_g(300\text{ K}) = (1.97 + 1.968 - 6.9x^2 + 9.1x^3)$  eV has been corrected to take account of the recommendations for the binary endpoints. When no further information is available, temperature dependence is incorporated using the recommended endpoints to fix the constant and linear terms at each temperature, and then use the quadratic and cubic terms of Peng *et al.* at all temperatures.

The same approach is recommended for zinc blend InAlN. The bowing (b) for cubic InAlN alloy, is equal to 1 [7].

## 2. Implementation of the Simulation Method

For our study we use the Monte Carlo method of simulation because it is the most appropriate for this work. It takes into account all the parameters of alloys for different molar fractions and it gives us the possibility to change the temperature, the electron concentration and the electric field. It allows us to have a good results about the velocity, the mobility and other results.

This method offers the possibility to reproduce the various microscopic phenomena observed in semiconductor materials. It is to monitor the behavior of each electron subjected to an electric field in real space and in the wave-vector space.

The software used in this method allows performing two basic functions. The first function can be used to calculate probabilities from the usual expressions. The second helps determine the instantaneous quantities defined on a set of electrons (energy, speed, position) by the so-called Self Scattering procedure [3] for which the free flight times are distributed over all electrons.

The implementation of this method was initially adopted by Kurosawa [4] and later improved by others [5]. It is based on a drawing of lots process of interactions sustained by the free carriers during their movement in the compound, from probability laws. It consists to follow the behavior of each electron in real space and in wave-vectors space [6].

Consider an electron which owns energy  $\Sigma(t)$ ,

wave-vector  $k(t)$ , and which is placed in  $r(t)$ . Under action of an applied electric field  $E(r, t)$ ; its interaction and exchange of energy with the lattice, and the deviation of its trajectory by impurities; this will modify its energy, its wave-vector and its position. Using the mechanic and the electrodynamics laws; we determine the behavior of each electron, in time and space. To be more realistic:

- 1 We statistically study possible energy exchanges between electrons, modes of lattice vibration and impurities; this allows us to calculate the probability of these interactions and their action on both electron energy and wave-vector.
- 2 We assume that these interactions are instantaneous. We can move electrons in free-flight under the only effect of electric field, between two shocks. The free-flight time is determined by the drawing of lots. When interaction takes place, we determine its nature by the drawing of lots. In this case, the electron energy and the electron wave-vector are modified. This results in a change of electrons distribution; we then calculate the electric field that results, at enough small time intervals, to assume it constant between two calculations [8]–[9]–[10].

We consider a simplified model of three isotropic and non parabolic bands. The wave-vector and energy of the electron are related by using (3) [11]:

$$\hbar^2 K^2 / (2m^*) = \varepsilon(1 + \alpha \varepsilon) \quad (3)$$

Where  $m^*$  is their effective mass in the  $\Gamma$  valley,  $\hbar k$  denotes the magnitude of the crystal momentum,  $\varepsilon$  represents the electron energy, and  $\alpha$  is the nonparabolicity factor of the considered valley, given by (4) [11]:

$$\alpha = (1/E_g)(1 - (m^*/m_0)) \quad (4)$$

Where  $m_e$  and  $E_g$ , denote the free electron mass and the energy gap, respectively.

$m_e = 0.21m_0$  for AlN, and  $m_e = 0.11m_0$  for InN [11].

The longitudinal  $V_l$  and transverse  $V_t$ , acoustic velocities [12]–[13]–[14]–[15] are calculated by using (5) and (6) (where  $\rho$  is the density of material, and  $C_{ij}$  are elastic constants):

$$V_l = (C_l / \rho)^{1/2} \quad (5)$$

$$V_t = (C_t / \rho)^{1/2} \quad (6)$$

The constants,  $C_l$  and  $C_t$ , are combinations of elastic constants and calculated by using (7) and (8):

$$C_l = (3C_{11} + 2C_{12} + 4C_{44}) / 5 \quad (7)$$

$$C_t = (C_{11} - C_{12} + 3C_{44}) / 5 \quad (8)$$

The general procedure for implementing the software consists of three basic steps:

- Reading the data file of different material parameters.
- Implementing the software.
- Providing output files containing the probability

values of various interactions and the averages of some quantities (energy, speed, population of valleys ...).

Over time, the behavior of the electrons in the conduction band results from the action of the external applied electric field as well as from their various interactions inside the crystal lattice. Here, the elastic and inelastic dispersions are considered.

$$E_{In_xAl_{1-x}N}^g = x X E_{InN}^g + (1-x) X E_{AlN}^g - 1.13 x(1-x) \quad (9)$$

### 3. Results and Discussion

The Monte Carlo simulation method was used to study the electron transport in bulk cubic  $In_xAl_{1-x}N$  compound, and the doping concentration was set to  $10^{17} \text{ cm}^{-3}$ . The scattering mechanisms included in our simulation were: the acoustic phonon, the polar and non-polar optical phonon (equivalent and non-equivalent inter-valley), the ionized impurities, and the piezoelectric scattering. Specifically, the electron drift velocity versus the applied electric field was studied for different molar fractions of indium ( $x = 0, x = 0.2, x = 0.5, x = 0.6, x = 0.8$ , and  $x = 1$ ), at various temperatures. The results are illustrated in figures 2 to 6.

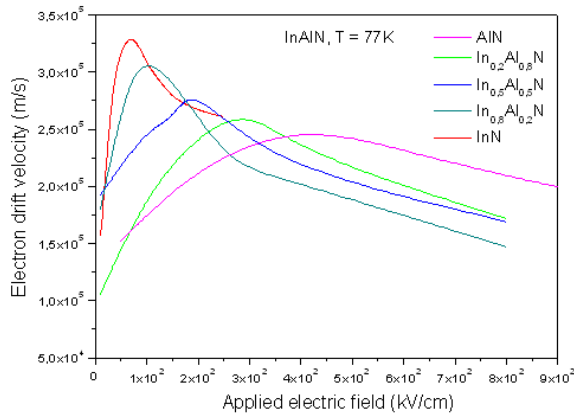


**Figure 2.** The electron drift velocity versus the applied electric field within  $In_xAl_{1-x}N$ , for different mole fractions of indium, at  $T = 77K$ .

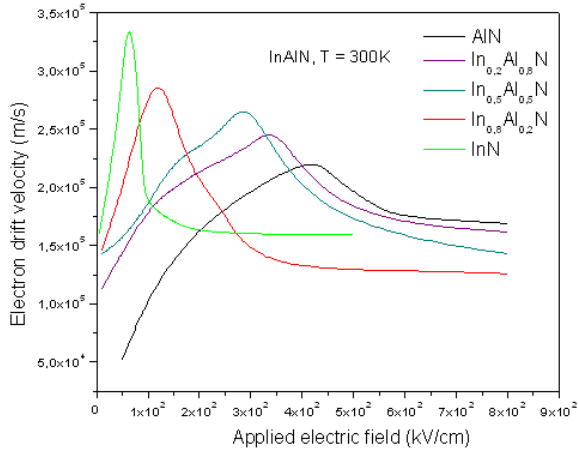


**Figure 3.** The electron drift velocity versus the applied electric field within  $In_xAl_{1-x}N$ , for different mole fractions of indium, at  $T = 300K$ .

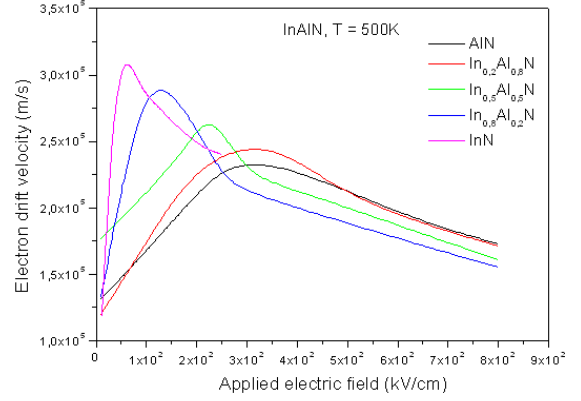


**Figure 4.** The electron drift velocity versus the applied electric field within  $In_xAl_{1-x}N$ , for different mole fractions of indium, at  $T = 500K$ .

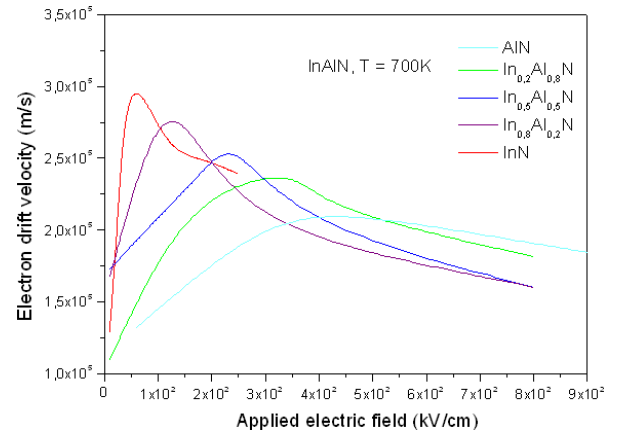


**Figure 5.** The electron drift velocity versus the applied electric field within  $In_xAl_{1-x}N$ , for different mole fractions of indium, at  $T = 700K$ .

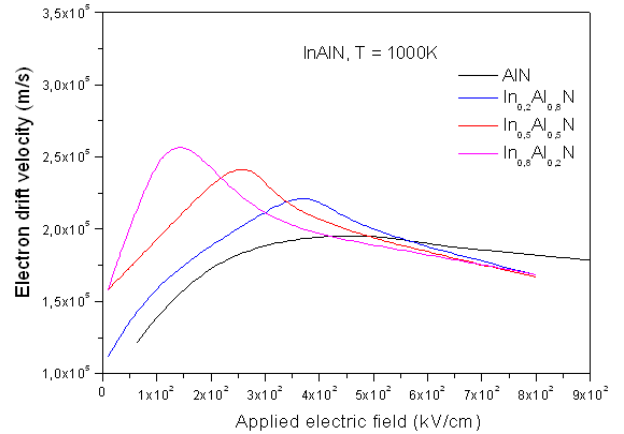


**Figure 6.** The electron drift velocity versus the applied electric field within  $In_xAl_{1-x}N$ , for AlN,  $In_{0.2}Al_{0.8}N$ ,  $In_{0.5}Al_{0.5}N$ , and  $In_{0.8}Al_{0.2}N$ .

When the indium mole fraction rises, the speed increases first and then gradually decreases; this can be explained as follows:

As the energy between  $\Gamma$  and L valleys and the effective mass of electrons in the central valley decrease, the electrons acquire a higher mobility and a higher speed until the applied field attains a critical value, which makes the electrons reach their maximum velocity. At this point, they are transferred to the upper valley where their population

and their effective mass increase, and consequently the inter-valley collisions raise. Due to all this, their velocity begins to decrease until saturation.

For all temperatures, when the indium mole fraction increases, the overshoot of the electrons increases; however the critical field shifts to lower fields, and the saturation velocity decreases and is eventually obtained for an electric field less than or equal to 800 kV/cm.

When the temperature is very low, the energy of thermal agitation ( $3/2 k_B T$ ) becomes much smaller than the energy of polar optical phonon ( $\hbar\omega_0 = 91.2$  meV).

At  $T = 77$  K, which is the temperature of liquid nitrogen, the energy of thermal motion does not exceed 9.96 meV. For low energy electrons, acoustic phonon collisions and optical phonon absorptions dominate. In both cases, the density of phonons is very small, and the interaction probabilities are very low. This temperature corresponds to the best electron velocity.

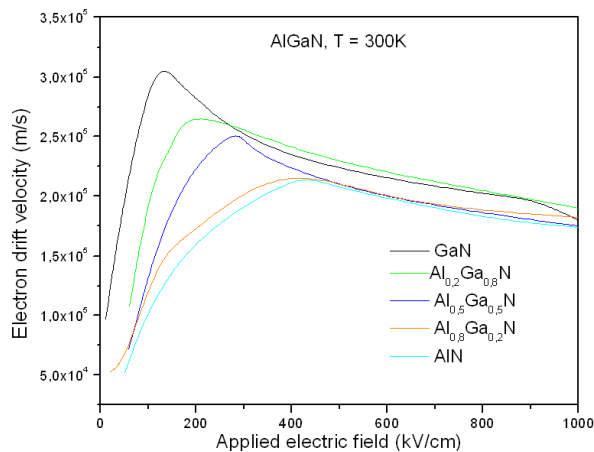


**Figure 7.** The electron drift velocity versus the applied electric field within  $Al_xGa_{1-x}N$ , for different mole fractions of aluminum, at  $T = 300$  K.

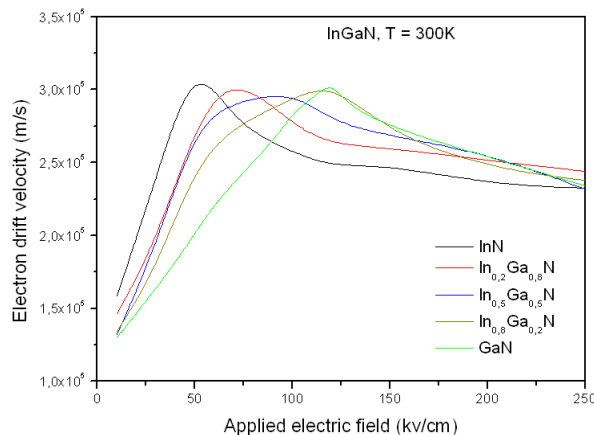


**Figure 8.** The electron drift velocity versus the applied electric field within  $In_xGa_{1-x}N$ , for different mole fractions of indium, at  $T = 300$  K.

Electron scattering is dominated by collisions of acoustic phonons, ionized impurities, and absorption of polar optical phonons which are removed at very low temperatures; this leads to better velocity and mobility.

When the temperature increases, the electrons acquire

higher kinetic energies; they move faster and collide with other atoms, thus transferring their energies. This causes a decrease in the number of free electrons.

For low electric fields, and temperatures less than or equal to 300 K, the impurity dispersion dominates and the speed increases. At higher temperatures, the hump disappears because the collisions of polar optical phonons dominate, while those of impurities decrease. For large fields, the scattering is dominated by polar optical phonon collisions, with low temperature dependence.

For comparison, the same calculation is done at 300 K for AlGaIn and InGaIn alloys; the results are shown in Figures 7 and 8, respectively.

We compare the electron velocity for the three ternaries at  $T = 300$  K and  $x = 0.5$ .

- For InAlN, the overshoot is around  $2.6 \times 10^5$  m/s for a critical field of about 284 kV/cm. The saturation velocity is approximately equal to  $1.4 \times 10^5$  m/s for a field equal to 800 kV/cm.
- For AlGaIn, the overshoot is around  $2.5 \times 10^5$  m/s for a critical field of about 282 kV/cm. The saturation velocity is approximately equal to  $1.75 \times 10^5$  m/s for a field equal to 1000 kV/cm.
- For InGaIn, the overshoot is around  $2.98 \times 10^5$  m/s for a critical field of about 99 kV/cm. The saturation velocity is approximately equal to  $2.3 \times 10^5$  m/s for a field equal to 500 kV/cm.

Within the InGaIn alloy, the electron drift velocity is higher but the saturation field is relatively smaller than that of InAlN.

Within AlGaIn, the electron drift velocity is smaller compared to that of InAlN, but the saturation field is much higher.

The InAlN alloy exhibits more advantages. Indeed, the addition of an In molar fraction increases the electron drift velocity, and the addition of an Al molar fraction increases the electric field at which the velocity saturation occurs.

When compared, our results are found to be in good agreement with those of reference [16].

## 4. Conclusion

InN, AlN and their alloys, constitute a major research area in solid state electronics for analog microwave applications. AlN and  $In_xAl_{1-x}N$  alloys with large Al concentrations exhibit several advantages. Such advantages are their high breakdown voltage which gives high output impedances due to the large bandgaps, their high saturation velocity, their high linearity, their resistivity to electromagnetic pulses, their chemical stability and high temperature stability.

However, for InN and InAlN alloys with large In concentrations, the gap is relatively small but the electrons can still reach very high speeds for low electric fields. Cubic alloys have a strong potential for optoelectronics, particularly in the far ultraviolet. However, it will be necessary to determine clearly the nature of the gap for high concentrations of aluminum. In addition, the epitaxial layer

quality is still quite low compared to those of hexagonal nitrides. The development of optoelectronic applications, based on cubic nitrides, needs a better control of the growth process; this is relatively difficult because of the nature of the metastable cubic phase and the lack of homogeneous cubic SiC substrates of good quality.

## References

- [1] Vurgaftman I, Ram-Mohan L R and Meyer J R 2001 *J. Appl. Phys.* 89 5815
- [2] Rosen G, *Matériaux pour l'Optoelectronique, Traite EGEM serie Optoelectronique*, tome 7, (Hermes Science Publications), Paris, 2003
- [3] K. Kubota, Y. Kobayashi, and K. Fujimoto, *J. Appl. Phys.* 66, 2984 -1989
- [4] J. Zimmermann, étude par la méthode de Monte Carlo des phénomènes de transport électronique dans le Silicium de type N en régimes stationnaire et non stationnaire. Application à la simulation des composants submicroniques, Thèse de doctorat d'état, U.de Lille 1, 1980.
- [5] T. Kurosawa, *Journal of the physical society of Japan*, supplement 21 (1966) 424
- [6] P. J. Price, *IBM Journal of Research and Development*, Vol 17 (1973) 39
- [7] O. Mouton, J. L. Thobel, and R. Fauquemberg "Monte Carlo simulation of high-field electron transport in GaAs using an analytical band structure model", *J. Appl. Phys.*, 74 (10) (1993)
- [8] Fabrice Enjalbert, thesis of doctorat, "Etude des hétérostructures semi-conductrices III-nitrides et application au laser UV pompé par cathode à micropointes," University of Grenoble 1, 2004.
- [9] Pugh S. K, Dugdale D. J, Brand S and Abram R.A, "Electronic structure calculation on nitride semiconductors," *Semicond. Sci. Technol*, vol 14, 1999, pp. 23–31.
- [10] Y. Zhang et al., "Anomalous strains in the cubic phase GaN films grown on GaAs (001) by metalorganic chemical vapour deposition," *J. Appl. Phys.*, vol. 88, N° 6, 2000, pp. 3762–3764.
- [11] Stephen K. O'Leary, Brian E. Foutz, Michael S. Shur, Lester F. Eastman, "Steady-State and Transient Electron Transport within the III–V Nitride Semiconductors, GaN, AlN, and InN," *A Review J Mater Sci: Mater Electron*, vol. 17, 2006, pp. 87–126.
- [12] R. Castagné, J. P. Duchemin, M. Gloanie, Ch. Rhumelhard, "Circuits intégrés en arsenic de gallium, Physique, technologie et conception," *Rev. Masson*, 1989.
- [13] N. Garro, A. Cros, A. Garcia, A. Cantarero, "Optical and vibrational properties of self-assembled GaN quantum dots," *Institute of Materials Science, University of Valencia*, 2007.
- [14] A.F.M. Anwar, Senior Member, Shangli Wu, and Richard T, Webster, "Temperature dependent transport properties in GaN, Al<sub>x</sub>Ga<sub>1-x</sub>N, and In<sub>x</sub>Ga<sub>1-x</sub>N semiconductors," *IEEE Transactions on Electron Devices*, vol. 48, No 3, March 2001, pp. 567–572.
- [15] A. Hamdoune, N. Bachir, Effects of Temperature and Concentration of Indium within Bulk Cubic In<sub>x</sub>Ga<sub>1-x</sub>N: Calculation of Steady State Electron Transport by Method of Monte Carlo Simulation, *International Journal of Computer and Electrical Engineering*, Vol. 2, No. 5, October, 2010, 1793-8163.
- [16] Rezaee Rokn-Abadi; Steady-state and transient electron transport within bulk ternary nitride semiconductors including GaInN, AlGaIn and AlInN using a three-valley Monte Carlo method; *M. Indian Journal of Science and Technology*; Vol. 3 No. 8 (Aug 2010).